Photographic aureole measurements and the validity of aerosol single scattering

R. D. McPeters and A. E. S. Green

A refined photographic system for solar aureole measurements is described in which a neutral density filter occulting disk blocks the direct sunlight. Experimental data for solar aureoles are presented for several wavelengths from 309 nm to 640 nm and solar zenith angles of up to 88°. The results are compared with a modified single scattering calculation that includes corrections for Rayleigh multiple scattering, attenuation by ozone, ground reflection, and spherical atmosphere geometry and, at 309 nm, are compared with a Monte Carlo multiple scattering calculation. Useful analytic functions for the aerosol size distribution and for the molecular, ozone, and aerosol height distributions are given. Our near sunset calculation represents an intermediate step between single scattering and full multiple scattering for a Rayleigh–ozone–aerosol atmosphere. We show that aerosol multiple scattering may not be ignored at large solar zenith angles and long wavelengths.

I. Introduction

Daytime skylight consists partly of light scattered by air molecules and partly of light scattered by aerosols. In the solar aureole the light scattered by aerosols predominates; hence, in a study directed toward determining the characteristics of atmospheric aerosols we might well concentrate on this region of the sky.

We have developed[1] a photographic technique for measuring the intensity distribution of scattered light in the solar aureole. Direct sunlight enters the camera only after passing through a neutral density four external occulting disk so that the sun and the surrounding aureole are at approximately the same intensity. Careful densitometric measurement of the film gives accurate ratios of aureole light intensity to direct solar intensity.

To interpret our aureole measurements we use a modified single scattering calculation which, for most cases, incorporates the major multiple scattering corrections. For accuracy the calculation uses spherical earth geometry at large solar zenith angles and includes the ground albedo contribution to sky brightness. A semiempirical correction factor for Rayleigh multiple scattering based upon the Coulson-Dave-Sekera (CDS) numerical tables is included to increase accuracy at short wavelengths. However, the use of only single aerosol scattering restricts us to the study of low to moderate aerosol optical depth data.

The authors are with the University of Florida, Gainesville, Florida 32611.

Received 29 January 1976.

II. Experimental Measurements

Photographic film offers several advantages over photoelectric detectors that are most widely used in studies of atmospheric sky brightness. The major advantage is the rapidity and ease with which data may be taken. In a single $\frac{1}{30}$-sec exposure with a 50-mm lens, we record sky brightness at high resolution over a large area of sky (26° by 38°). The modulation transfer function for Panatomic-X film shows that it will resolve a spatial frequency of 30 cycles/mm. This corresponds to 2-min. of arc resolution, at a 90% response level, which means that one frame represents a 900,000 point array of data stored very compactly and available for analysis at any future date. The photographic aureole system is simple, portable, and independent of any power supply. Thus, aureole data may be taken at a variety of locations with a minimum of preparation. While photoelectric systems have an advantage of linear response over a wide dynamic range, they require a cumbersome mechanical and electronic system, and extreme care must be taken to eliminate scattered and diffracted light. The requirements for our photographic system are much less stringent since the scattered light is minimized by our obscuring disk, and the diffracted light is localized and can be avoided in analysis. Finally, film, in conjunction with an analysis based upon accurate characteristic exposure–density curves, has a reasonably large dynamic range (3 decades). Films are available that are sensitive from about 1100 nm down to 270 nm and even lower for low gelatin emulsions.

We photograph the sky light near the sun using a Nikon FTN 35-mm camera mounted on a World War II searchlight guidance unit that may be finely con-

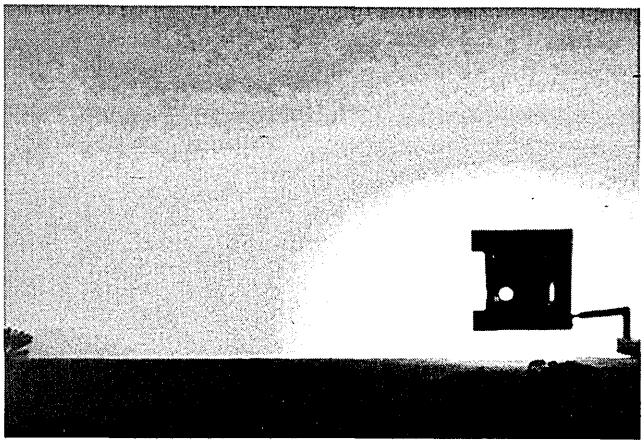

Fig. 1. An example of an aureole photograph showing aureole and the attenuated solar disk.

trolled in azimuth and elevation. Normally a 50-mm lens is used to cover a large area of the sky, but for finer resolution we use a 135-mm lens, which covers only 10° × 15°. Either lens gives accurate information to within 1° of the sun's center. We photographed the uv solar aureole at 309 nm using a one element 108-mm quartz lens at $f/14$.

In all cases direct sunlight, which is about 10^4 times brighter than the surrounding aureole, is blocked from entering the lens by a neutral density 4 occulting disk mounted about 1 m in front of the lens. The occulting disk blocks the sun and about ¾–1° of the solar aureole. A typical aureole photograph is shown in Fig. 1. The filter is an inconel coated (reflection type) quartz neutral density filter with a Callier Q factor of about 1.005. The sun appears on the film attenuated by the filter, giving us a calibration point for calculation of the ratio of aureole intensity to direct sunlight intensity.

Filters are used to limit the spectral range of each aureole photograph. Interference filters centered at 309 nm, 425 nm, and 850 nm are each of 10-nm halfwidth. Broadband Wratten absorption filters, 98, 99, and 92, centered at 430 nm, 540 nm, and 640 nm, respectively, have halfwidths of about 30 nm. The 92 red filter is actually a long pass filter, but the film sensitivity drops to zero at 690 nm to give an effective filter cutoff at this point. We normally use Panatomic-X because of its low speed, fine grain, and high gamma. However, we have tried a number of different film in our work, including Tri-X, High Speed Infrared, and Spectrum Analysis 1. With each roll of aureole film, we develop a sensitometer strip: film on which a series of precisely known exposures have been made with a tube sensitometer. For greatest accuracy the sensitometer strip is matched in processing, spectral quality, and exposure time to the original aureole exposures. The sensitometer strips are used to define an analytic characteristic HD curve[2] which we use to obtain the intensity of points in the aureole from the densities of the corresponding points on the film. The $\cos^4$ factor applied to correct for off-axis intensity variation was found to be accurate within 2% with our filter–lens–camera combination within 12° of the optical axis.

III. Single Scattering Calculation

A theoretical calculation of sky brightness assuming that light reaching the ground has scattered only once produces quite good agreement with observation under conditions of small aerosol optical depth and aureole scattering angles.

The intensity I of monochromatic light observed in the direction (θ,ϕ) zenith angle and azimuth angle of line of sight, when the sun is at zenith angle θ_s, is given by

$$I_\lambda(\theta_s,\theta,\phi) = \int_0^\infty [\beta_R(h,\lambda)P_R(\psi) + \beta_M(h,\lambda)P_M(\psi)] \times I_0 T_1 T_2 ds, \quad (1)$$

where I_0 is the solar intensity, and h is the altitude during integration over path s. The $P(\psi)$ are the scattering phase functions for the scattering angle ψ relative to the sun. The relative altitude distributions as expressed by the $\beta(h)$, the volume scattering coefficients, are usually assumed invariant: changes in aerosol optical depth and ozone thickness are made by varying the altitude distribution uniformly.

T_1 and T_2, the transmission factors from the scattering volume to the ground and from the top of the atmosphere to the scattering volume, are given by

$$T_2(h) = \exp\left\{-\int_0^\infty [\beta_R(s) + \beta_M(s) + \beta_{0z}(s)]ds\right\}, \quad (2)$$

$$T_1(h) = \exp\left\{-\int_0^L [\beta_R(l) + \beta_M(l) + \beta_{0z}(l)]dl\right\}. \quad (3)$$

Here s is the path followed by the sunlight in reaching the scattering volume, and l is the path (of length L) followed in reaching the ground. Blättner *et al.*[3] show that for solar zenith angles of less than 90°, refraction need not be included. The altitude integrations were carried out in 1-km increments to a maximum altitude of 80 km. We found this integration step size to give excellent results when used with Simpson's rule, since

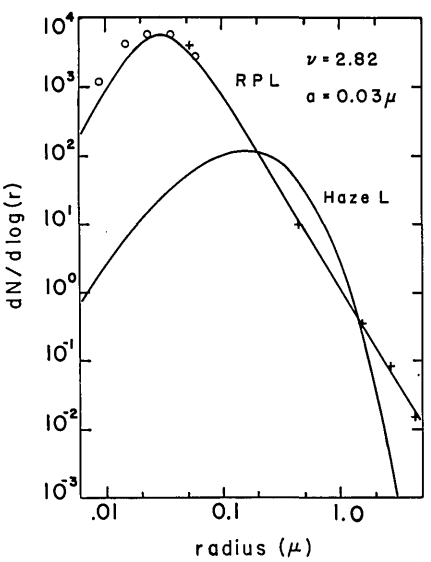

Fig. 2. Size distribution measurements of Junge compared with our regularized power law and Deirmendjian's Haze L distribution.

doubling the number of integration points caused only a 0.01% variation.

Our objective in performing this calculation is to compare calculated aureole intensities with aureole intensities obtained by our photographic technique. A key feature of the photographic method is that the solar disk (attenuated by a neutral density filter) is recorded along with the aureole, and it is more accurate to obtain the ratio of aureole to solar disk intensities than to attempt to obtain absolute intensities directly from the photograph. Once this ratio is accurately known, reference to the direct solar intensity at ground level measured by a solar radiometer[4] allows the absolute aureole intensities to be inferred. The intensity of light for the sun's disk is calculated by

$$I_s(\lambda,\theta_s) = [1/(\Delta\Omega_s)] \exp(-\tau_0 \sec\theta_s), \tag{4}$$

where τ_0 is the total optical depth at ground level, and $\Delta\Omega_s$ is the solid angle subtended by the sun. Integration over wavelength gives the aureole pattern corresponding to our measurements.

$$\frac{\bar{I}(\theta_s,\theta,\phi)}{\bar{I}_s(\theta_s)} = \frac{\int_{\Delta\lambda} T_F(\lambda)S_F(\lambda)I_\lambda(\theta_s,\theta,\phi)d\lambda}{\int_{\Delta\lambda} T_F(\lambda)S_F(\lambda)I_s(\lambda,\theta_s)d\lambda}, \tag{5}$$

where T_F is the filter transmission, and S_F is the relative film sensitivity.

IV. Aerosol Size Distribution

The most prominent feature of the natural aerosol size distribution as first described by Junge[5] is the power law decrease in number density with increasing particle radius. Here the term size distribution refers to the radius-number distribution $n(r)$: the number of particles per cubic centimeter per unit radius range centered at r, where r is the particle radius in microns. Junge[5] found that a cumulative distribution $N(r)$ for continental aerosols is described by

$$dN(r) = cr^{-\nu}d(\log r). \tag{6}$$

This corresponds to the size distribution

$$n(r) = dN(r)/dr = (C/\ln_e 10)r^{-(\nu+1)}. \tag{7}$$

This distribution is frequently used directly in calculations with an externally imposed lower cutoff (about 0.01 μm, to avoid singularity problems at $r = 0$. The exponent ν is found to range between 2.5 and 4.0.

In our analysis of light scattering, we avoid the singularity by use of the regularized oversize distribution

$$N(r) = N_0/[1 + (r/a)^\nu], \tag{8}$$

which corresponds to the size distribution

$$n(r) = N(0)\frac{\nu}{a^\nu}\frac{r^{\nu-1}}{[1 + (r/a)^\nu]^2}. \tag{9}$$

This size distribution vanishes at $r = 0$ and is identical with the Junge distribution when $r \gg a$. The parameter ν thus corresponds to that of Junge, and a is approximately the radius at which the number frequency is maximum. In Fig. 2 we compare data points found by Junge[5] with Deirmendjian's standard Haze L distribution and our regularized power law distribution adjusted to $\nu = 2.8$ and $a = 0.03$ μm. Our distribution is used with an upper cutoff radius r_{max} large enough that the Mie phase function in the 1–12° range is not sensitive to its value.

While the simple regularized power law is adequate to describe a normal size distribution, a bimodal distribution can be described by summing two terms of this form [Eq. (8)].

V. Analytic Altitude Distributions

Realistic altitude distributions for air, ozone, and aerosols must be used to produce accurate sky brightness patterns for large solar zenith angles. We have found analytic functions that match observed altitude distributions for all three components quite well. The altitude distribution of air is approximately exponential, but it is more accurately represented by a form of generalized distribution function[6]

$$N_R(h) = N_0\frac{(1+\alpha)^2\exp(h/h_0)}{[\alpha + \exp(h/h_0)]^2}, \tag{10}$$

where h is the altitude in kilometers, $h_0 = 6.42$ km is a scale height, $\alpha = 0.312$ is a shape parameter, and N_0 is the ground level molecular number density. A comparison of the altitude distribution calculated using Eq. (10) with the altitude distribution given by Elterman's[7] 1968 standard atmosphere is shown in Fig. 3.

We assume that the aerosol size-altitude distribution is separable, and we represent the altitude distribution as a weighted sum of two generalized distribution functions. The first term has the scale height of 1.18 km and the shape constant of 0.0661; the second term, which is included to represent the high altitude aerosol component, has the scale height of 3.3 km, a shape parameter of 80, and a weight of 1.27×10^{-3}. The sum of the two distributions is multiplied by $N_M(0)$, the aerosol number density at ground level as determined by a particle counter for instance. The ozone altitude distribution is represented by a generalized distribution function representing the stratospheric layer and an

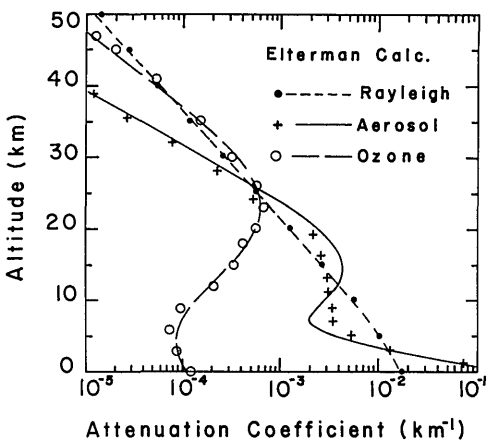

Fig. 3. Altitude distributions of the 500-nm Rayleigh, aerosol, and ozone attenuation coefficients measured by Elterman (1968) compared with analytic functions.

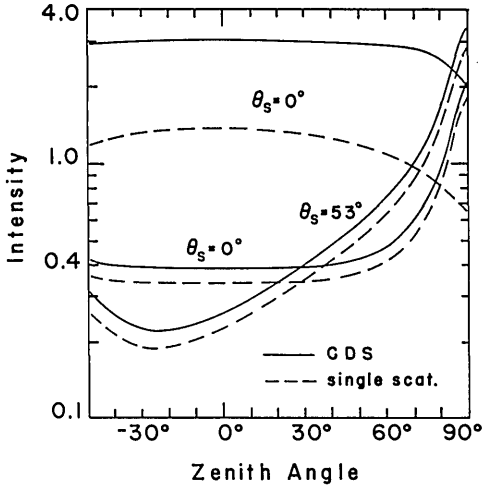

Fig. 4. Rayleigh multiple scattering as calculated by Coulson *et al.* compared with single scattering. The two upper curves are for 309 nm, the four lower curves for 500 nm.

exponential term that describes the tropospheric ozone. For convenience, we write it in the form

$$N_{0z}(h) = \frac{N_{s0}\exp[(h-h_p)/h_{0s}]}{\{1+\exp[(h-h_p)/h_{0s}]\}^2} + N_{t0}\exp(-h/h_{0t}), \quad (11)$$

where $N_{s0} = 0.2139$, $h_p = 23.0$ km, $h_{0s} = 4.44$ km, $N_{t0} = 0.0096$, and $h_{0t} = 5.78$ km.

VI. Ground Albedo Correction

Since light traveling at a large zenith angle is close to the ground over a large part of its path, we felt that including light reflected from the ground would increase the accuracy of the near-sunset aureole calculation. Bauer and Dutton[8] measured ground albedo in Wisconsin from an airplane for different seasons and terrain and found that wooded terrain in summer had an average albedo of 0.15–0.20. The flat, sandy soil of Florida might be expected to have a slightly higher albedo, so we used a value of 0.25 in our calculation except for the 309-nm calculation, for which an albedo of 0.0 was used. Using a local albedo as high as 0.25 we found the contribution from ground reflection to be small reaching appreciable values (5%) only for very clear air. Albedo was not as important at large zenith angles as we originally expected. For a pure Rayleigh atmosphere ground reflection can contribute as much as 25% in increased light, but for the computations for the 2 days studied here, our calculations only yielded about 3% increase.

VII. Rayleigh Multiple Scattering Correction

Multiple scattering is important at short wavelengths, large optical depths, large scattering angles, and large zenith angles. Accurately representing multiple scattering requires the use of a multistream calculation such as that of Mudgett and Richards[9] or a Monte Carlo calculation such as that used by Plass and Kattawar.[10] Since our objective is to model atmospheric scattering as closely as possible without resorting to a full multiple scattering formalism, we add a correction term corresponding to the multiple scattering of the Rayleigh component only. Coulson *et al.*[11] have published tables giving the scattered radiation including all orders of multiple scattering for a plane parallel Rayleigh atmosphere for various solar zenith angles, scattering angles, albedos, and wavelengths.

To find the correction factors, we reproduced their tables for single scattering and took the ratio of multiple to single scattering intensities. In Fig. 4 we compare the multiple scattering results and the single scattering results for two different sun angles and two different wavelengths. One notes that the multiple scattering and single scattering sky brightness patterns are very similar, the difference being primarily one of magnitude. To a good approximation, then, the results of the Coulson, Dave, and Sekera (CDS) calculation can be matched to the solar aureole over the 15° or so in the vicinity of the sun by multiplying the single scattering result by a constant correction factor. The variation of the CDS factor with wavelength and solar zenith angle is approximately described by the function

$$F(\theta_s,\lambda) = 1 + \frac{1}{\mu_s^{1/4}}\left(\frac{330}{\lambda}\right)^4, \quad (12)$$

where $\mu_s = \cos(\theta_s)$.

The importance of the CDS factor depends on the relative optical depth of the aerosol component. Our calculations of the solar aureole for 540 nm and for large aerosol optical depth, 0.32 for 26 April 1975, gave an increase in aureole intensity of 0.1–1.4% for scattering angles of zero and 15°, while for a small aerosol optical depth, 0.023 for 22 November 1974, we obtained an increase of 0.6% and 9.6% for the same scattering angles. The correction factor is less important at small scattering angles because the strong forward peaking of the aerosol scattering makes the Rayleigh component relatively less important. The CDS factor is largest for short wavelengths, being 2 at 312 nm. Thus, at uv wavelengths a true multiple scattering calculation should probably be made.

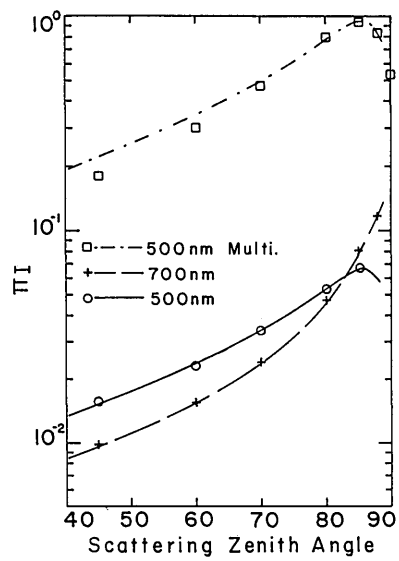

Fig. 5. Sky brightness for the sun at $ZA = 88°$ for a Rayleigh–ozone atmosphere as calculated by Blättner *et al.* (points) compared with results of our modified single scattering calculation.

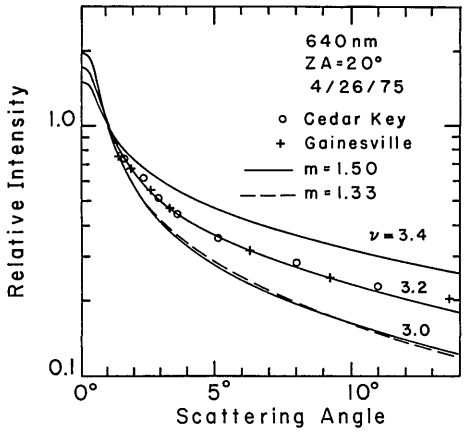

Fig. 6. Measured aureole intensity along the almucantar compared with calculations for three ν variations in the aerosol size distribution.

Blättner *et al.*[3] recently made a Monte Carlo multiple scattering calculation for a Rayleigh and ozone atmosphere and spherical geometry. As a check on the accuracy of our work we compare the results of our calculation with no aerosols to those of Blättner *et al.* in Fig. 5. These results are for an extreme case, a solar zenith angle of 88°. The single scattering results agree quite well, and, as can be seen, our CDS factor produces good agreement with their multiple scattering result for the region near the sun.

VIII. Comparison of Measured and Calculated Solar Aureoles

We attempt to infer the size distribution based on the scattering pattern of the solar aureole and the aerosol optical depth as measured by the solar radiometer, yet this represents only a limited amount of information. Our technique is to constrain the aerosol size distribution models to those that are physically reasonable in light of the cumulation of prior investigations. Other investigators handle the problem of inversion to find the size distribution without assuming a size distribution model. The Backus-Gilbert inversion technique[12] or that of Twitty[13] may be capable of establishing the size distribution with no *a priori* assumptions. But it has generally been found that noisy data present difficulties to strict numerical inversion methods.

Our modified single scattering calculation models the experiment as accurately as possible, so to determine the aerosol size distribution we calculate the expected aureole for an array of size distribution parameters [the ν and a parameters in Eq. (8) or (9)] and compare the results with the measured aureole data. The sensitivity of the aureole to the ν parameter is shown in Fig. 6. A solar radiometer measurement of the aerosol optical depth fixes the amount of aerosol used in the calculation, and we use the average monthly ozone thickness for our location.

We have chosen to normalize most of the graphs to unity at a 1° scattering angle in order to emphasize the shape of the aureole rather than its magnitude. This renders errors in scale due to error in measurement of the density of the occulting disk or in measurement of the aerosol optical depth less important. Moreover, this reduces the importance of having the correct aerosol index of refraction since, as shown in the comparison of calculations with $m = 1.33$ and 1.50 in Fig. 6, the shape of the aureole is very nearly the same in the two cases. As is shown, the effect of varying the size distribution parameters is large on such a graph. The data of Fig. 6 were taken in Gainesville, Florida, which is about 60 miles (96 km) inland, and on Cedar Key, Florida, which is just offshore in the Gulf of Mexico. The data show that the aerosols at the two locations on this day were nearly identical and not continental vs maritime.

The calculations for Fig. 6 were made with a size distribution peaking near $a = 0.03$ μm. Because the submicron particles contribute little to the inner aureole, little difference is seen whether $a = 0.03$ μm or $a = 0.10$ μm is used in the calculation. However, values of a larger than this place the peak of the size distribution into the effective light scattering domain, and the calculation is more sensitive to changes in a. The value we chose is in agreement with counter measurements that indicate that the size distribution peaks in the 0.01–0.10-μm range usually. Moreover, if the size distribution peaks at a larger radius, the allowable ground level particle density decreases rapidly, since large particles are very effective attenuators. Typical particle counter measurements in Gainesville show about 10^4 particles/cm^2 and an average background mass loading of about 30 μg/m^2. The size distribution used for this day, which was a day of large aerosol optical depth, gives a ground level number density of 4.4×10^4 particles/cm^2 and 75 μg/m^2, numbers consistent with Gainesville particle counter and high volume sampler measurements.

In Fig. 7 we plot experimental aureole data for 22 November 1974 at three wavelengths on an absolute scale, the ordinate being the ratio of aureole intensity to attenuated direct sun intensity. The large ratio for 430 nm is caused by the higher density of the occulting disk in this wavelength region. The inversion of the 640-nm and 540-nm ratios is somewhat unusual, but is

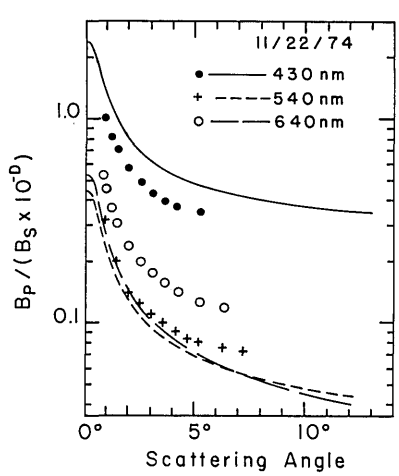

Fig. 7. The ratio of aureole intensity to attenuated solar intensity at three wavelengths compared on an absolute scale with results of modified single scattering calculation.

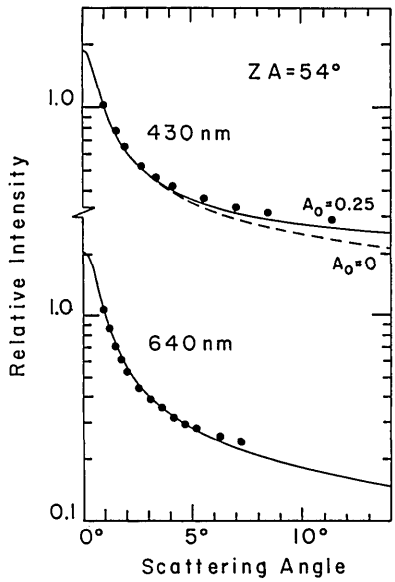

Fig. 8. Normalized aureole intensities along the almucantar compared with calculated results at two wavelengths.

consistent with the fact that the 700-nm aerosol optical depth was higher than that at 600 nm. Such behavior is frequently seen and is caused by a non-Junge aerosol size distribution, possible bimodal. The fits on an absolute scale could be improved by varying the index of refraction or adding additional components to the aerosol size distribution, but varying the size distribution outside the size range that affects the shape of the aureole would obscure the effects we are interested in: the effects of ground albedo and the suitability of our multiple scattering correction factor.

In Fig. 8 we show aureoles for 22 November for a zenith angle of 54° (air mass 1.70) at two wavelengths. Good fits to the data for this date were obtained with a size distribution of $\nu = 2.9$ and $a = 0.03\ \mu$m. The importance of the albedo correction is shown in Fig. 8, the 430-nm aureole. The calculations for albedoes of 0.0 and 0.25 do not differ in the inner aureole; but at 10° and greater, the fit to the data is significantly better for an albedo of 0.25.

Figure 9 shows the solar aureole for the same date and wavelengths, but for a solar zenith angle of 75° and along a vertical cut below the sun (toward the horizon). The two sets of data shown for the 430-nm aureoles are in each case from different negatives, one made with a 50-mm lens and the other made with a 135-mm lens. The calculated aureole predicts an increase in sky brightness near the horizon at 640 nm, while the data show only a small increase at the horizon. This discrepancy could be caused by our use of Elterman's model atmosphere. These aureoles were measured on an exceptionally clear day, so that the 0–3-km aerosol layer probably did not contain as large a fraction of the total aerosol as predicted by this model, and the low level aerosols are responsible for the near-horizon brightness increase.

Figure 10 shows sunset aureoles, vertical cuts above the sun, which is itself only 2° above the horizon. The photographs here were not intended for vertical cut analysis, so the 430-nm aureole negative was analyzed along a vertical cut adjacent to the sun, about 3° away horizontally. Hopefully this cut will still give much the same aureole pattern except for the first few degrees. The agreement between data and calculation was rather poor for the 540-nm case because of the neglect of aerosol multiple scattering. The agreement in the 430-nm aureole is better because Rayleigh scattering, which has been corrected for multiple scattering, is relatively more important.

Calculations for the 309-nm aureole are shown for a

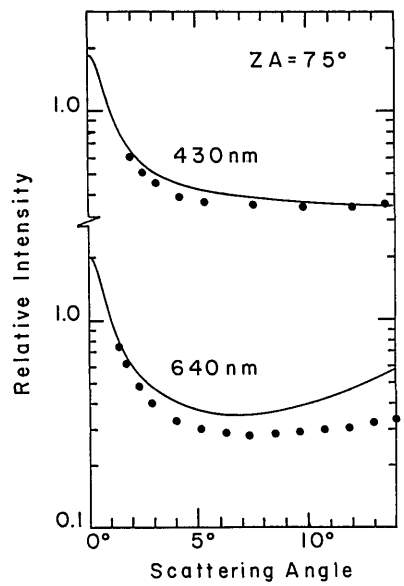

Fig. 9. Normalized aureole intensity below the sun (ZA = 75°) at two wavelengths compared with calculation.

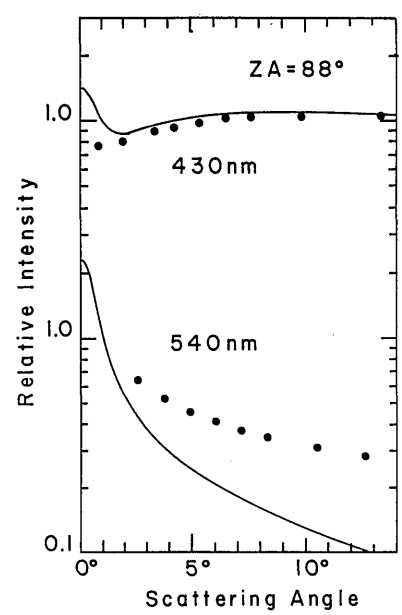

Fig. 10. Normalized aureole intensity above the sun (ZA = 88°) compared with calculation to show the importance of aerosol multiple scattering.

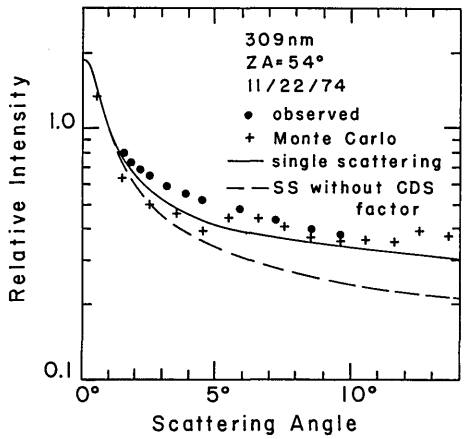

Fig. 11. Normalized uv aureole intensities along the almucantar compared with modified single scattering calculation, with and without the CDS Rayleigh multiple scattering correction factor, and compared with a Monte Carlo full multiple scattering calculation.

solar zenith angle of 54° in Fig. 11. As might be expected, because of the dominance of the Rayleigh scattering process at 309 nm, the single scattering calculation including the CDS correction factor does a much better job of fitting the observed solar aureole than does the single scattering calculation shown without the correction factor.

For comparison, we used a Monte Carlo program[14] based on the programs of Plass and Kattawar to match our atmosphere model and size distribution but with a plane parallel atmosphere. Channels 1° in width were used in order to resolve the aureole; unfortunately, use of such a large number of channels produces large statistical fluctuations in the individual channels.

The Monte Carlo and modified single scattering calculations agree with each other quite well; they agree with each other better than they do with the data. Considering the relative costs, the modified single scattering calculation does a good job of modeling the solar aureole even in the uv when compared with the Monte Carlo calculation.

IX. Conclusion

Many others have studied the solar aureole, but our technique of measuring the sky to sun intensity ratio through use of film and a neutral density occulting disk is, we believe, unique. The sunset sky brightness has recently been calculated for realistic atmosphere models. We concentrate on the near-sun sky brightness and attempt to match actual sunset aureoles to a calculation that includes multiple Rayleigh scattering but only single scattering from aerosols. Comparison of data and calculation indicates that at short wavelengths the solar aureole is governed by Rayleigh multiple scattering, but at longer wavelengths aerosol multiple scattering must be included in a calculation of the sunset solar aureole.

The use of analytic rather than numerical models is a strong technique that we believe should be more widely used in atmospheric optics problems. As we have shown, a few rather simple analytic forms can be applied quite flexibly to reasonably smooth distributions; only highly structured distributions, such as the extraterrestrial solar flux or the spectral ozone absorption coefficients, require numerical modeling.

The modified single scattering calculation that we have developed is sufficiently flexible to match a wide range of atmospheric conditions and in many cases offers significant improvement over a simple single scattering calculation.

This work was supported in part by The National Science Foundation under Grant ATM75-21962.

References

1. A. E. S. Green, A. Deepak, and B. Lipofsky, Appl. Opt. **10,** 1263 (1971).
2. A. E. S. Green and R. McPeters, Appl. Opt. **14,** 271 (1975).
3. W. G. Blättner, H. G. Horak, D. G. Collins, and M. B. Wells, Appl. Opt. **13,** 534 (1974).
4. R. Sutherland, R. McPeters, G. Findley, and A. E. S. Green, J. Atmos. Sci. **32,** 427 (1975).
5. C. E. Junge, J. Meteorol. **12,** 13 (1955).
6. A. E. S. Green and P. J. Wyatt, *Atomic and Space Physics* (Addison-Wesley, Reading, Mass., 1966).
7. L. Elterman, "UV, Visible, and IR Attenuation for Altitudes to 50 km," AFCRL Environmental Research Paper 285 (1968).
8. K. G. Bauer and J. A. Dutton, J. Geophys. Res. **67,** 2367 (1962).
9. P. S. Mudgett and L. W. Richards, Appl. Opt. **10,** 1485 (1971).
10. G. N. Plass and G. W. Kattawar, Appl. Opt. **7,** 415 (1968).
11. K. L. Coulson, J. V. Dave, and Z. Sekera, *Tables Related to Radiation Emerging From a Planetary Atmosphere with Rayleigh Scattering* (University of California Press, Berkeley, 1960).
12. E. R. Westwater and A. Cohen, Appl. Opt. **12,** 1340 (1973).
13. J. T. Twitty, J. Atmos. Sci. **32,** 584 (1975).
14. D. R. Furman, T. Mo, and A. E. S. Green, to be published in J. Atmos. Sci. **33,** 537 (1976).